EVALUATING FARGO-MOORHEAD FLOOD RISK MANAGEMENT PROJECT USING THE HYDROLOGIC AND WATER QUALITY SYSTEM

A Thesis

by

XIAOHAN MEI

Submitted to the Office of Graduate and Professional Studies of
Texas A&M University
in partial fulfillment of the requirements for the degree of

MASTER OF SCIENCE

Chair of Committee,	Raghavan Srinivasan
Committee Members,	Clyde Munster
	Raghupathy Karthikeyan
Intercollegiate Faculty Chair,	Ronald Kaiser

December 2017

Major Subject: Water Management and Hydrological Science

ABSTRACT

Spring floods in the Red River basin generated from melting snow have increasingly affected the Fargo-Moorhead metropolitan region of North Dakota and Minnesota within recent decades, causing serious economic damage and disturbance to the local community. Various local and federal government agencies have come together to formulate a flood management project mainly utilizing water diversion to protect the Fargo-Moorhead urban area from future floods. Major structural measures that alter the surface water flow regime would take place under the current project proposal. This study applied the Hydrologic and Water Quality System to set up the study watershed, covering the upper portion of the Red River basin with its outlet located in Fargo. The Soil and Water Assessment Tool Calibration and Uncertainty Procedures were used to perform sensitivity analysis, model calibration, and model validation on a chosen set of hydrologic input parameters. Results from one of the general circulation models, the Geophysical Fluid Dynamics Laboratory's global coupled carbon-climate earth system model with vertical coordinates based on density, were coupled with the hydrologic model to set up predictive simulations to evaluate climate change impacts on the study watershed. A flood diversion channel was added into the predictive simulations in the form of point-source water extraction. The time durations for the predictive simulations were divided into two decade-long sections, 2026 to 2035 and 2036 to 2045, which represent the short- to medium-terms following project construction completion. Results of the predictive simulations indicate a significant increase in streamflow for the entire

simulation time span under both RCP4.5 and RCP8.5 climate change scenarios. Meanwhile, the implementation of a diversion channel near the Fargo-Moorhead urban area would have a strong impact on the flow regime of the Red River at Fargo, where a streamflow pattern with lower average discharge and lower flow variability is predicted for the flood-diversion-included simulations. The inclusion of the flood diversion channel in the model also significantly reduces the occurrence of large-magnitude streamflow events.

ACKNOWLEDGEMENTS

I would first like to thank my academic advisor and committee chair, Dr. Srinivasan. He has steered this thesis project in the right direction and has always answered my questions and given me instructions with great patience and extraordinary expertise. I would also like to thank my committee members, Dr. Munster and Dr. Karthikeyan, for their guidance and support throughout this research.

My thanks also go to the chair of the water program, Dr. Kaiser, as well as other department faculty and staff who have been very helpful during my study at Texas A&M University. In addition, I am thankful to my friend Gang Zhao, who gave me very useful advice for the climate change projections in my research.

I am sincerely grateful for the Water Management & Hydrological Sciences Graduate Student Scholarship, which hugely benefited me by reducing my personal financial stress during my past two years in graduate school.

Finally, I am always grateful to my parents for their caring and encouragement.

CONTRIBUTORS AND FUNDING SOURCES

Contributors

This work was supervised by a thesis committee consisting of Professor Raghavan Srinivasan of the Department of Ecosystem Science and Management and Professor Clyde Munster and Professor Raghupathy Karthikeyan of the Department of Biological and Agricultural Engineering.

The data analyzed for Chapter II was obtained from the USGS National Water Information System.

All other work conducted for the thesis was completed by the student independently.

Funding Sources

There are no outside funding contributions to acknowledge related to the research and compilation of this document.

NOMENCLATURE

CF	Change Factor
CFM	Change Factor Methodology
CMIP5	Coupled Model Intercomparison Project Phase 5
CV	Coefficient of Variation
DEM	Digital Elevation Model
EIS	Environmental Impact Statement
EPA	Environmental Protection Agency
ESM	Earth System Model
FEMA	Federal Emergency Management Agency
F-M	Fargo-Moorhead
GCM	General Circulation Model
GFDL	Geophysical Fluid Dynamics Laboratory
GIS	Geographic Information System
HAWQS	Hydrologic and Water Quality System
HRU	Hydrologic Response Unit
HUC	Hydrologic Unit Code
IPCC	Intergovernmental Panel on Climate Change
MNDNR	Minnesota Department of Natural Resources
NOAA	National Oceanic and Atmospheric Administration
NSE	Nash-Sutcliffe Efficiency

PBIAS	Percent Bias
PRISM	Parameter-Elevation Regressions on Independent Slopes Model
R^2	Coefficient of Determination
RCP	Representative Concentration Pathway
RGU	Responsible Government Unit
SUFI2	Sequential Uncertainty Fitting Version 2
SWAT	Soil and Water Assessment Tool
SWAT-CUP	SWAT Calibration and Uncertainty Procedures
USACE	United States Army Corps of Engineers
USGS	United States Geological Survey

TABLE OF CONTENTS

Page

ABSTRACT ii

ACKNOWLEDGEMENTS iv

CONTRIBUTORS AND FUNDING SOURCES v

NOMENCLATURE vi

TABLE OF CONTENTS viii

LIST OF FIGURES ix

LIST OF TABLES x

CHAPTER I INTRODUCTION AND LITERATURE REVIEW 1

1.1 Flood Damage and Management 1
1.2 Red River Flooding in the Fargo-Moorhead Metropolitan Region 2
1.3 Fargo-Moorhead Flood Risk Management Project 3
1.4 Objective 4

CHAPTER II METHODOLOGY 6

2.1 SWAT and HAWQS 6
2.2 Study Area Description and HAWQS Setup 8
2.3 SWAT-CUP and SUFI2 Procedures 10
2.4 Sensitivity Analysis 12
2.5 Model Calibration and Validation 15
2.6 Predictive Simulation Setup 25

CHAPTER III RESULTS AND DISCUSSION 36

3.1 Results 36
3.2 Discussion 43

CHAPTER IV SUMMARY AND CONCLUSIONS 46

REFERENCES 48

APPENDIX A 59

LIST OF FIGURES

Page

Figure 1. Location of the study area: the upper Red River basin at the border area of Minnesota, North Dakota, and South Dakota. 9

Figure 2. Subbasins of the study area and United States Geological Survey (USGS) stream gages used for calibration and validation (USGS 05051522: Red River of the North at Hickson, ND; USGS 05053000, Wild Rice River near Abercrombie, ND; USGS 0505400,: Red River of the North at Fargo, ND)... 10

Figure 3. Measured versus simulated discharge during the model calibration period. 22

Figure 4. Measured versus simulated discharge during the model validation period. 23

Figure 5. Two periods (1980 to 1989 and 1990 to 1999) of simulated and measured discharge of the Red River of the North at Fargo, ND. 36

Figure 6. Predicted Daily Streamflow of the Red River at Fargo from 2026 to 2035 under four possible scenarios (RCP4.5 with diversion channel, RCP4.5 without diversion channel, RCP8.5 with diversion channel, RCP8.5 without diversion channel). 37

Figure 7. Predicted Daily Streamflow of the Red River at Fargo from 2036 to 2045 under four possible scenarios (RCP4.5 with diversion channel, RCP4.5 without diversion channel, RCP8.5 with diversion channel, RCP8.5 without diversion channel). 38

Figure 8. The number of days from (a) 2026 to 2035 and (b) 2036 to 2045 with 10-, 50-, 100-, and 500-year flood magnitudes under four projected discharge scenarios (RCP4.5 with flood diversion, RCP4.5 without flood diversion, RCP8.5 with flood diversion, and RCP8.5 without flood diversion). 42

LIST OF TABLES

Page

Table 1. Selected model parameters for sensitivity analysis. 14

Table 2. Selected Parameters for Model Calibration 19

Table 3. Calibration and validation statistic results for the study watershed. 21

Table 4. Output hydrology parameters of calibration and validation periods. 24

Table 5. Monthly CF for precipitation, in percentage. 31

Table 6. Monthly CF for temperature, in degC. 32

Table 7. Adjusted climate variability parameters [Arnold et al., 2012]. 33

Table 8. Statistical results of the baseline and projected daily streamflow scenarios for 2026 to 2035 and 2036 to 2045, units in m^3/s. 39

Table 9. FEMA Peak flow and stage data of USGS gage at Fargo, data obtained from Clay County Flood Insurance Study [Minnesota Department of Natural Resources, 2016] 42

Table 10. Percent change of the number of different-magnitude flood events when diversion channel is included. 43

Table 11. Land use distribution of the study watershed. 59

Table 12. T-test results for the sensitivity analysis. 61

Table 13. The number of days of different flood recurrence intervals of the Red River at Fargo. 62

CHAPTER I

INTRODUCTION AND LITERATURE REVIEW

1.1 Flood Damage and Management

Floods have been a constant threat to human society throughout recorded history. As population pressure and human activities continue to grow in many parts of the world in the contemporary era, as well as alternating global climate patterns, a growing trend of flood magnitude and frequency has been observed in many riverine systems [*Dutta et al.*, 2006]. The term "flood damage" often refers to all the negative effects created by flooding, normally including loss of human life, damage to private property and public infrastructure, and detrimental impact on local ecological systems. In most situations, the total amount of socioeconomic damage cannot be accurately quantified due to the complex nature of a flooding event and the many indirect effects it may incur [*Messner and Meyer*, 2006].

In many cases, flood damage caused by a specific event can become the driving force for formulating flood management policy and projects. Flood risk management often involves actions at two different levels: managing the existing flood protection system or planning and building a new system. The former option focuses on taking actions based on the currently available hydrological structures and intends to minimize the impact of flood disasters through mitigation efforts. Specific measures in this category include analyzing potential flood risk, providing reliable early warnings, maintaining hydrological structures like dikes and reservoirs, and preparing for

emergency disaster response such as evacuation or rescue. However, when the existing system becomes inadequate to prevent potential flooding events due to factors such as land use change or climate change, the latter level of action is taken to construct a new structural system for flood protection [*Plate,* 2002].

1.2 Red River Flooding in the Fargo-Moorhead Metropolitan Region

The Red River of the North originates from the confluence of Bois de Sioux and Otter Tail Rivers at Wahpeton, North Dakota, draining parts of the states of South Dakota, Minnesota, and North Dakota and flowing northward for approximately 394 miles within the United States before reaching the Canadian province of Manitoba [*Stoner et al.,* 1993]. Climate factors in the region are the driving force for the diverse flow regime at the Red River. The Red River basin generally experiences cold, frozen winters and warm summers, with an annual mean temperature of about 40 degF. The main stem of the Red River often experiences flooding events during the snow-melting period of a year, with its tributaries having similar flooding characteristics [*Miller and Frink,* 1984]. Observed discharge data in recent decades suggest a tendency toward earlier flooding for the snowmelt-derived Red River due to climate warming [*Stewart et al.,* 2005].

The Fargo-Moorhead (F-M) metropolitan region of North Dakota and Minnesota is located within the regular flood plain of the Red River, with the river itself separating the city of Fargo on the west bank from the city of Moorhead on the east bank. Throughout recorded history, the F-M metropolitan region has been frequently affected

by spring floods in late March and early April caused by snowmelt of the Red River basin [*U.S. Army Corps of Engineers,* 2011]. The F-M metropolitan area is the largest urban area in the sparsely populated North Dakota, with a population of approximately 200,000. It is the region's social and economic center. Recent hydrologic records of the Red River have shown an increasing trend in flooding frequency and magnitude. The Minnesota Department of Natural Resources (MNDNR) has estimated the average annual economic flood damages in the F-M metropolitan area to be more than 51 million USD [*Minnesota Department of Natural Resources,* 2016]. Although no direct human casualty has been recorded in recent flooding events, the heavy economic loss and high risk of future flooding events have made flood management more imperative.

1.3 Fargo-Moorhead Flood Risk Management Project

Historically, many responsible government units (RGUs) from the states of North Dakota and Minnesota have overlapped in the their efforts surrounding water management and conservation of the Red River [*Hearne*, 2007]. To reduce possible damage to the local communities from future floods, the United States Army Corps of Engineers (USACE), MNDNR, and many other agencies at the local and state levels have worked together to propose a flood management project that would primarily benefit the F-M urban area.

The initial-draft feasibility report for the flood management project prepared by the USACE discussed a few alternative plans, including the construction of flood barriers, diversion channels, and flood storage facilities, as well as taking nonstructural

measures by continuing the current warning and emergency response system without additional engineering projects. More particularly for the diversion channel, the USACE proposed a few options with different diversion capacities and at various geological locations, each emphasizing a distinct priority [2011].

While various flood management designs and alternative projects were described and evaluated extensively in the initial-draft feasibility report, the RGUs working on the project planning came to the conclusion that nonstructural measures are insufficient for mitigating potential flood risk; therefore, the project formulated in the final environmental impact statement (EIS) involves constructing a combination of different hydrological structures, including an approximately 30-mile-long diversion channel on the west side of the F-M urban area, an additional embankment along the Red River and a few of its local tributaries, control structures for diverting flow from the Red River into the diversion channel, a staging area to the south of the urban area for flood retention purposes, and ring levees for protecting communities located within the staging area [*Minnesota Department of Natural Resources*, 2016].

1.4 Objective

This study intends to use the Hydrologic and Water Quality System (HAWQS) to set up a hydrological model for the upper portion of the Red River basin, to calibrate and validate the model using available flow records of the modeling river basin, and to couple the model with climate projections from the Coupled Model Intercomparison

Project Phase 5 (CMIP5) to predict future flood regimes under different climate change scenarios after the completion of the F-M flood risk management project.

More specifically, the objective of this study includes exploring answers to the following questions:

1). How will the hydrological process of the Red River change under different future climate projections?

2). What is the effectiveness of the planned flood prevention structures, particularly the diversion channel, in affecting the flow regime of the Red River and reducing future flood magnitude?

This thesis is organized into the following sections: Chapter 2 explains the methodology and contains a description of the study area and model, sensitivity analysis of model parameters, calibration and validation of the model, integration of climate projections, and setup of the predictive simulations. Chapter 3 includes results and discussion and presents the results of the projections and analysis results and limitations. Chapter 4 is the conclusion, which summarizes the study.

CHAPTER II

METHODOLOGY

2.1 SWAT and HAWQS

The Soil and Water Assessment Tool (SWAT) is a physical-based, continuous-time model developed for the assessment of water quality and quantity in large river basins with varying soils, land uses, land cover types, and management practices [*Arnold et al.*, 2012]. Watershed is divided into a few subbasins in the SWAT model; the model further groups lands with homogeneous slope, soil type, and land cover type into hydrologic response units (HRUs), which may not be spatially continuous [*Licciardello et al.*, 2011; *Tuppad et al.*, 2011]. The development of the SWAT model has spanned the last three decades, with new functions and routines continuously added to the model; the current SWAT model has been widely applied to water, sediment, agricultural chemicals, and contaminant yields in complex systems [*K Abbaspour et al.*, 2015; *Gassman et al.*, 2007]. Moreover, a significant amount of SWAT input data contains spatial information, so the SWAT model can be integrated with a geographic information system (GIS). For example, the popular ArcSWAT interface was developed based on the ArcGIS platform, which hugely enhances usability of the SWAT model [*Jayakrishnan et al.*, 2005; *Olivera et al.*, 2006; *Srinivasan and Arnold*, 1994].

SWAT performs simulations based on user-defined input data [*Neitsch et al.*, 2011]; however, the process of setting up a new SWAT project can be cumbersome and time-consuming, especially when the size of input data is large, normally associated with

large watershed size or high resolution of the input digital elevation model (DEM), and computational resources are limited.

As an alternative to ArcSWAT, HAWQS is a public-domain, web-based hydrological modeling system developed and maintained by Texas A&M University Spatial Sciences Laboratory and the United States Environmental Protection Agency (EPA). HAWQS uses the core engine of SWAT and has an interactive web interface that provides its users with preloaded maps and input data, which significantly reduces its initialization procedures [*Fant et al.*, 2017]. In addition to reducing initialization procedures, HAWQS can continue with its tasks on its server when the user web interface is closed and can inform the user by email when tasks are completed [*Yen et al.*, 2016].

In the project setup phase, HAWQS creates project watershed based on user-identified downstream watershed; the downstream watershed can be identified by selecting its hydrologic unit code (HUC). Data resolution in HAWQS can be switched between HUC8, HUC10, and HUC12. Similar to SWAT, HAWQS enables its users to limit the amount of HRUs by setting threshold levels on soil type, land use, and slope class, either through percentage or area. After the project setup phase, the land use distribution and soil and slope classes for the project watershed are summarized into an output table or chart. More specific scenarios with user-defined weather dataset, simulation time duration, output time step, and SWAT model version can be created after the project setup [*Spatial Sciences Laboratory Texas A&M AgriLife Research*, 2016].

2.2 Study Area Description and HAWQS Setup

A portion of the upper Red River basin was selected as the study area (Figure 1). The studied watershed covers parts of Minnesota, North Dakota, and South Dakota and was set up in HAWQS by selecting the most downstream subbasin, HUC 090201040504. The selected outlet subbasin overlaps the F-M metropolitan region, around which the flood risk management project would take place. The study watershed is located between 45.52˚ and 47.15˚ north latitude and 95.42˚ and 97.94˚ west longitude; it has a total area of 17,015.94 km^2 and is divided into 178 subbasins based on the selected data resolution of HUC12 (Figure 2). The original number of HRUs in the study watershed is 10,667, and after a threshold of 5% applied to land use, soil type, and slope class, the number of HRUs reduces to 2,801. Summary tables of land use and soil type distributions for the study watershed are generated by HAWQS after project setup procedures. It is mentioned in the literature that the land use type of the Red River basin is primarily agricultural, which makes up about 74% of the land area [*Stoner et al.*, 1993]. Similarly, the land use distribution output table from HAWQS suggests that corn and soybean are the dominant crop species for the study watershed, with the corn-soybean rotation fields covering about half of the study area, while deciduous forest, open water, and nonforested wetland are the major cover types apart from agricultural land (Table 11 in Appendix A). Major tributaries of the Red River of the North in this area include the Bois de Sioux River, Otter Tail River, and Wild Rice River of North Dakota. The Bois de Sioux River and Otter Tail River flow together at Wahpeton, North

Dakota, to form the Red River, while the Wild Rice River flows into the Red River approximately 7 miles south of the city of Fargo [*Stoner et al.*, 1993].

After delineating the study watershed, new project scenarios are created with specified essential information, including input weather dataset, simulation start and end date, the number of warmup years, and simulation time steps. In this study, the calibration and validation simulation was performed on a monthly time step, while the predictive simulation was performed on a daily time step.

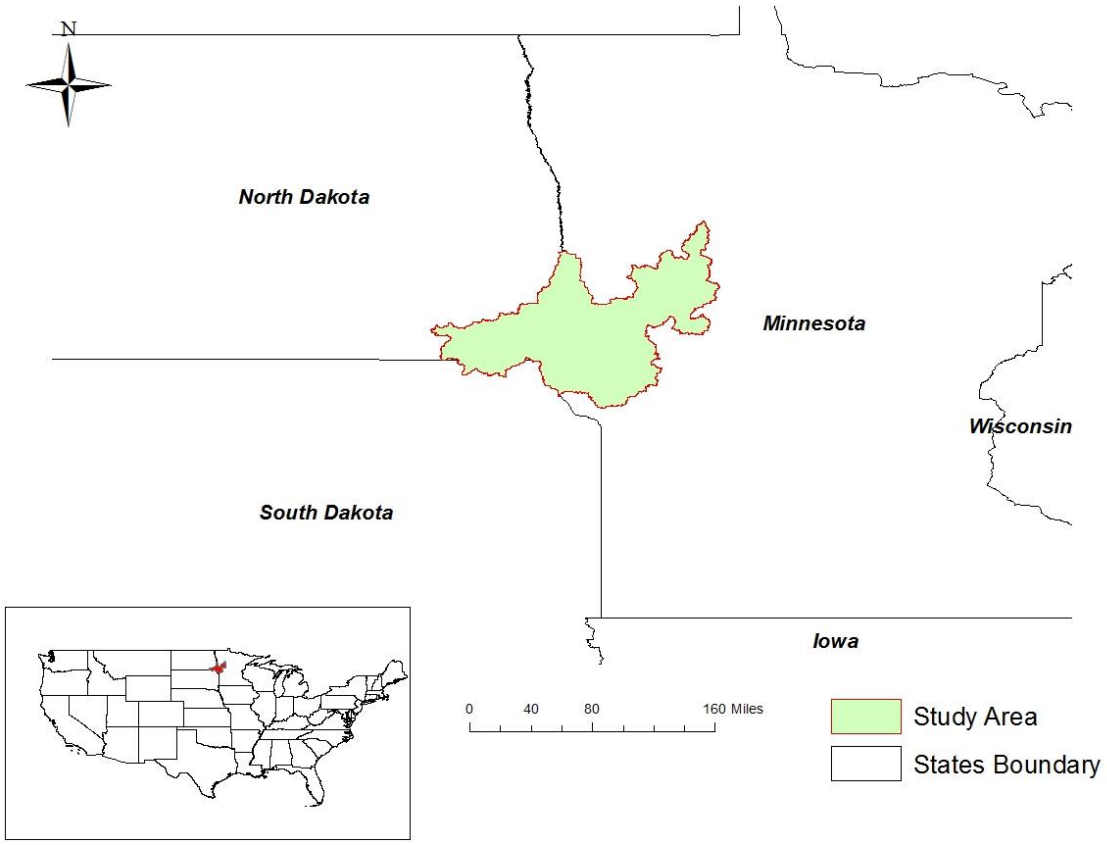

Figure 1. Location of the study area: the upper Red River basin at the border area of Minnesota, North Dakota, and South Dakota.

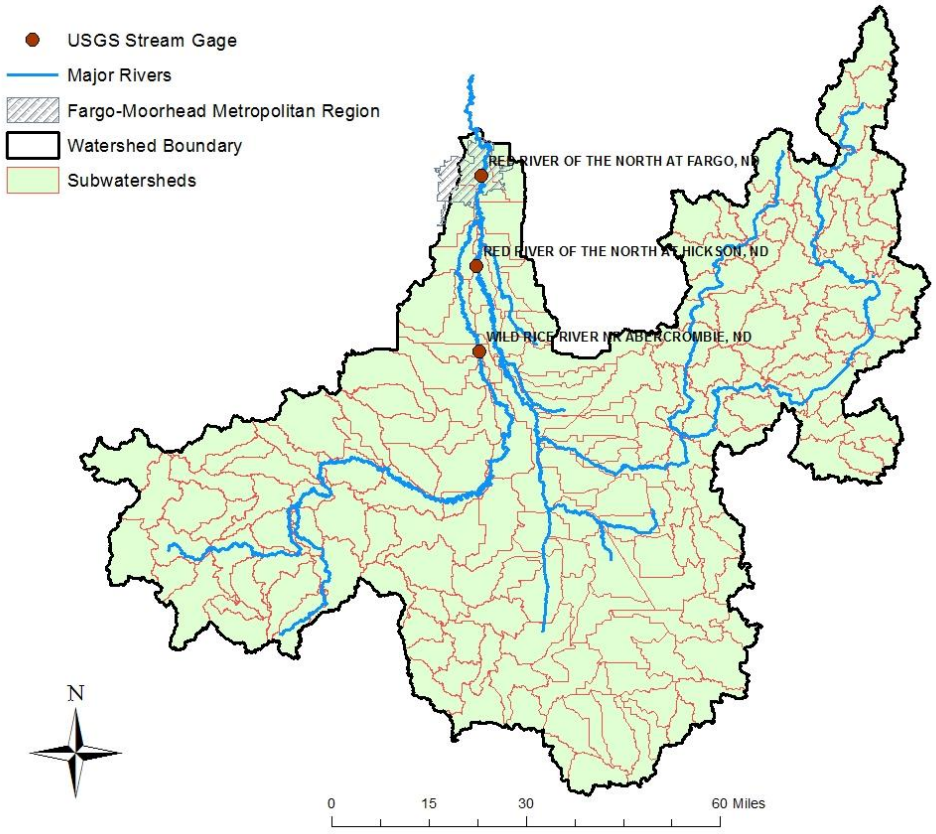

Figure 2. Subbasins of the study area and United States Geological Survey (USGS) stream gages used for calibration and validation (USGS 05051522: Red River of the North at Hickson, ND; USGS 05053000, Wild Rice River near Abercrombie, ND; USGS 0505400,: Red River of the North at Fargo, ND).

2.3 SWAT-CUP and SUFI2 Procedures

A new project scenario using climate data from the Parameter-Elevation Regressions on Independent Slopes Model (PRISM) and spanning from 1989 to 2010 was set up for model calibration and validation. The first two years of simulation were used as a warmup period, followed by data from 1991 to 2000 being used for the calibration phase and data from 2001 to 2010 being used for the validation phase. The simulation for the calibration phase was set on a monthly time step to reduce processing

time, given the example in the literature that calibrated parameters can be transferred across a temporal scale and can be used on a daily time step for predictive simulations [*Daggupati et al.*, 2015].

Project files created in HAWQS were linked to SWAT Calibration and Uncertainty Procedures (SWAT-CUP) for sensitivity analysis and calibration procedures. SWAT-CUP is a public-domain software package developed for sensitivity analysis, calibration, validation, and uncertainty analysis for SWAT models. SWAT-CUP can link a few different optimization algorithms to input SWAT models [*K C Abbaspour*, 2011] and can perform parallel processing on computers that have multiple central processing units (CPUs) with a purchased license [*Rouholahnejad et al.*, 2012]. A comparison between available optimization procedures was conducted by Yang et al., with results indicating that the Sequential Uncertainty Fitting Version 2 (SUFI2) procedure could reach good prediction uncertainty ranges with the smallest number of model runs, which is a significant advantage for computationally demanding models [*Yang et al.*, 2008].

The SUFI2 procedure was used for parameter optimization for the current project. Uncertainty of parameters in SUFI2 is expressed as uniformly distributed ranges, parameter uncertainties lead to model output uncertainties, and the output uncertainty is quantified using the 95% prediction uncertainty (95PPU), which is calculated at 2.5% and 97.5% of cumulative distribution obtained through Latin hypercube sampling [*K Abbaspour et al.*, 2006; *Schuol et al.*, 2008a]. Since the result of the SUFI2 procedure is expressed in 95PPU band, uncertainty in the optimization

process cannot be quantified using traditional indices such as the Nash-Sutcliffe Efficiency (NSE) or coefficient of determination (R^2) [*Rouholahnejad et al.*, 2012]. Therefore, two other indices, the *P*-factor and *R*-factor, are often used to quantify the quality of calibration performance. The *P*-factor represents the percentage of data bracketed by the 95PPU band and has a maximum value of 100%; the *R*-factor, on the contrary, is the average width of the band divided by the standard deviation of the corresponding measured variable. A *P*-factor approaching 100% indicates more measured data bracketed within the 95PPU band, while an *R*-factor approaching 0 indicates a narrower band [*K C Abbaspour et al.*, 2009]. The ideal outcome is to have the largest *P*-factor with the smallest *R*-factor; however in practice, the increment of *P*-factor is at the expense of a larger *R*-factor, so the optimization procedure often needs to seek the best trade-off between the two factors [*Schuol et al.*, 2008b].

2.4 Sensitivity Analysis

Sensitivity analysis is the procedure analyzing the change of model output due to the variation of model inputs; it is normally used to identify the parameters that have a significant impact on model output. The sensitive parameters identified through this procedure are comparatively more important during the following model calibration phase [*Chu and Shirmohammadi*, 2004; *Feyereisen et al.*, 2007; *Lenhart et al.*, 2002]. Two types of sensitivity analysis, global and one-at-a-time, are available in SWAT-CUP. One-at-a-time sensitivity analysis can only be performed for one parameter at a time, whereas global sensitivity analysis can be performed iteratively with a number of

simulations larger than 16 [*K C Abbaspour*, 2011], which is more convenient to conduct and was therefore applied in the current project.

A sensitivity analysis can be implemented through a variety of approaches. In SWAT-CUP, a t-test is performed to identify the significance of each parameter, and the larger the absolute value of the t-statistic and the smaller the p-value, the more sensitive a parameter is [*K C Abbaspour*, 2011]. Some previous studies have mentioned a lack of information in terms of SWAT's performance in simulating streamflow caused by snowmelt; they have pointed out that the SWAT model for these northern watersheds has better performance for simulations with longer time steps [*Ficklin and Barnhart*, 2014; *Lee et al.*, 2011; *Peterson and Hamlett*, 1998; *Qi and Grunwald*, 2005; *Wang and Melesse*, 2005]. Helpful information about SWAT parameters that affect snowmelt hydrology is mentioned in the literature [*Fontaine et al.*, 2002; *Omani et al.*, 2016]. For this project, 14 parameters were selected for sensitivity analysis (Table 1) [*Raghaven Srinivasan*, personal communication, June 30, 2017].

Table 1. Selected model parameters for sensitivity analysis.

Hydrology Input Parameter	Description
CN2	SCS runoff curve number for antecedent moisture condition II
ALPHA_BF	Base flow alpha factor (days)
GW_DELAY	Delay time for aquifer recharge (days)
GWQMN	Threshold depth of water in the shallow aquifer required for return flow to occur (mm H_2O)
GW_REVAP	Groundwater "revap" coefficient
REVAPMN	Threshold depth of water in the shallow aquifer for "revap" or percolation to the deep aquifer to occur (mm H_2O)
RCHRG_DP	Deep aquifer percolation fraction
SFTMP	Snowfall temperature (degC)
SMTMP	Snowmelt base temperature (degC)
SMFMX	Maximum melt factor on June 21 in northern hemisphere (mm H_2O $d^{-1}\,^{\circ}C^{-1}$)
SMFMN	Minimum melt factor on December 21 in northern hemisphere (mm H_2O $d^{-1}\,^{\circ}C^{-1}$)
TIMP	Snow temperature lag factor
SOL_AWC	Available water capacity of the soil layer (mm H_2O /mm soil)
ESCO	Soil evaporation compensation factor

An iteration with 20 simulations was performed on the selected parameters using SWAT-CUP; results for the sensitivity analysis were obtained from the output t-statistic and p-value (Table 12 in Appendix A).

2.5 Model Calibration and Validation

2.5.1 Goodness-of-Fit Indicators

The SUFI2 procedure uses *P*-factor and *R*-factor, which both describe the characteristic of the 95PPU band, to quantify the uncertainty of SWAT-CUP iteration; therefore, the solution of each iteration is the output parameter range. However, the SUFI2 procedure can also find the best set of parameters within the output ranges and can compute the best objective function value for a current iteration using traditional statistic indices [*K C Abbaspour*, 2011].

Eleven traditional statistic indices are available in the SUFI2 procedure for pairwise comparison of measured data and the best model prediction, among which three commonly used goodness-of-fit indicators, coefficient of determination (R^2), NSE, and percent bias (PBIAS), were selected for presenting statistical results of this study and are briefly discussed in the following section.

The coefficient of determination (R^2) is often used as a measure of precision in predictions for general linear models; in SWAT-CUP, R^2 can be represented by Equation 1:

$$R^2 = \frac{\left[\sum_i \left(Q_{m,i} - \overline{Q_m}\right)\left(Q_{s,i} - \overline{Q_s}\right)\right]^2}{\sum_i \left(Q_{m,i} - \overline{Q_m}\right)^2 \sum_i \left(Q_{s,i} - \overline{Q_s}\right)^2} \quad (1)$$

where Q is the variable, m and s stand for measured and simulated, respectively, and i stands for the i^{th} data point [*K C Abbaspour*, 2011]. R^2 is often used in searching for the regression equation between two sets of data; it has a value range from 0 to 1, and a larger R^2 indicates an increase in predictive precision [*Barrett*, 1974].

NSE is a dimensionless index widely applied in many hydrologic models; it is a normalized statistic and determines the magnitude of residual variance compared to measured data variance [*Nash and Sutcliffe*, 1970]. Some previous studies have suggested that NSE is better at evaluating model goodness-of-fit than R^2, mainly because R^2 is insensitive to additive and proportional differences between measured and simulated data; however, it has also been pointed out that NSE can be overly sensitive to extreme outliers because it squares the values of paired differences [*R Harmel et al.*, 2014; *R D Harmel and Smith*, 2007; *Qi and Grunwald*, 2005]. NSE can be represented by Equation 2:

$$NSE = 1 - \frac{\sum_i (Q_m - Q_s)_i^2}{\sum_i (Q_{m,i} - \overline{Q_m})^2} \quad (2)$$

where Q is the variable, *m* and *s* stand for measured and simulated, respectively, and *i* stands for the i^{th} data point [*K C Abbaspour*, 2011]. NSE ranges from –∞ to 1.0, with NSE = 1.0 representing the optimal fitting. A negative NSE value indicates that the mean observed value is a better fit compared to the simulated value [*Moriasi et al.*, 2007; *X Zhang et al.*, 2010; *X Zhang et al.*, 2009]. Furthermore, *Moriasi et al.* mentioned that NSEs between 0.0 and 1.0 are generally viewed as acceptable levels of model performance; however, an NSE larger than 0.50 is often viewed as the behavior

threshold for satisfactory model performance [*Daggupati et al.*, 2015; *Omani et al.*, 2016].

PBIAS measures the average tendency of simulated data to be larger or smaller than observations [*Gupta et al.*, 1999]. The model reaches optimal prediction with a PBIAS of 0.0, and a lower magnitude of PBIAS indicates a more accurate model prediction. Furthermore, positive values indicate that the model output underestimates the observation, while negative values indicate overestimation [*Gupta et al.*, 1999; *Moriasi et al.*, 2007]. PBIAS is calculated by Equation 3:

$$PBIAS = 100 * \frac{\sum_i (Q_m - Q_s)_i}{\sum_i Q_{m,i}} \quad (3)$$

where Q represents the variable, *m* and *s* stand for measured and simulated, respectively, and i stands for the i^{th} data point [*K C Abbaspour*, 2011]. While PBIAS can clearly indicate poor prediction accuracy, the value of PBIAS tends to vary more compared with previously mentioned indicators; meanwhile, it also varies more substantially between wet and dry years [*Moriasi et al.*, 2007]. An absolute value of PBIAS smaller than 25 is considered to be satisfactory for SWAT model calibration [*Daggupati et al.*, 2015; *Omani et al.*, 2016].

2.5.2 Model Calibration Procedure

Application of a multisite and multivariable method can significantly improve model calibration by highlighting the hydrological processes associated with spatial variation [*Cao et al.*, 2006; *X-s Zhang et al.*, 2008]. The current study sought to evaluate

a flood management project that considers discharge the major issue; therefore, discharge was used as the only variable in the calibration process. On the other hand, given the relatively large spatial extent of the study watershed, discharge data from three USGS gage stations were obtained for calibration and validation. The surface water gages include USGS 05054000, Red River of the North at Fargo, ND, USGS 05053000, Wild Rice River near Abercrombie, ND, and USGS 05051522, Red River of the North at Hickson, ND (Figure 2). The calibration and validation procedures were conducted in a monthly time step to reduce computational time in SWAT-CUP. Monthly average discharge for the three stations from 1991 to 2010 was obtained from the USGS National Water Information System (https://waterdata.usgs.gov/nwis/monthly/).

Among the 14 parameters selected for sensitivity analysis, 10 parameters with a comparatively larger impact on model output were selected for model calibration. Rank of parameter sensitivity and initial parameter adjustment range are presented in Table 2. Changes made to the parameters during the calibration procedure should follow their physical meaning, so for most parameters in Table 2, the existing parameter value is to be replaced by the given value; however, for parameters that have spatial variability, such as curve number or soil parameters, the often applied types of change are relative, which means multiplying the existing parameter value by 1 plus the given value, or absolute, meaning the given value is added to the existing parameter [*K C Abbaspour*, 2011].

Table 2. Selected Parameters for Model Calibration

Hydrology Input Parameter	Sensitivity Rank	File Extension	Method of Change	Value Range
CN2	1	.mgt	Relative	–0.1, 0.1
SMFMN	2	.bsn	Replace	0.0, 2.5
SOL_AWC	3	.sol	Relative	–0.05, 0.05
RCHRG_DP	4	.gw	Absolute	–0.05, 0.05
GWQMN	5	.gw	Absolute	–1000, 1000
ESCO	6	.hru	Replace	0.6, 0.95
SFTMP	7	.bsn	Replace	–2.0, 1.0
SMFMX	8	.bsn	Replace	2.5, 4.5
ALPHA_BF	9	.gw	Replace	–0.0, 1.0
TIMP	10	.bsn	Replace	–0.0, 1.0

NSE was used as the objective function for the calibration procedure with its behavior threshold set to 0.50. SUFI2 is an iterative procedure with each iteration containing a number of simulations; for this reason, the SWAT-CUP user manual recommends around 500 simulations for each iteration and repeating the iteration to find better statistical results; usually, less than five iterations is sufficient to reach an acceptable solution. However, the user manual also mentions that fewer numbers of simulations, 200 to 300 for instance, could be acceptable if a SWAT project is overwhelming for the available computational resource [*K C Abbaspour*, 2011]. For this project, four iterations, each with 300 simulations, were performed for the calibration

phase spanning from 1991 to 2000, in which output parameter ranges of an iteration were used to update the input parameter range of the next iteration. After the calibration procedure, the output parameter ranges of the last iteration were used as the input parameter ranges of model validation. In the meantime, the observed discharge data were updated to the years 2001 to 2010. Model validation was performed afterward through an iteration with 300 simulations making the above-mentioned changes.

2.5.3 Calibration and Validation Results

The objective of model calibration was reached, given that the overall output of objective function for both calibration and validation period are above the 0.50 behavior threshold. The weighted best NSE for the study watershed has the value 0.774 for the calibration period and 0.766 for the validation period (Table 3).

Table 3. Calibration and validation statistic results for the study watershed.

Period	Objective Function (NSE)	USGS Gage	P-factor	R-factor	Coefficient of Determination (R2)	NSE	PBIAS
Calibration (1991 to 2000)	0.774	05051522	0.52	0.42	0.82	0.74	19
		05054000	0.56	0.4	0.86	0.86	7.1
		05053000	0.22	0.36	0.77	0.72	–31.8
Validation (2001 to 2010)	0.766	05051522	0.43	0.41	0.76	0.72	5.6
		05054000	0.47	0.39	0.76	0.76	0.7
		05053000	0.34	0.31	0.84	0.82	–1.8

Meanwhile, results from the goodness-of-fit indicators show that model prediction reached satisfactory levels for each calibrated subbasin during both the calibration and validation periods [*Moriasi et al.*, 2007]. During the calibration period, the Red River of the North at the Fargo (USGS 05054000) gage station, which is also the outlet of the entire study watershed, reached the best statistical results among the three calibrated sites. However, for the validation period, the Wild Rice River near Abercrombie (USGS 05053000) showed the best statistical performance (Table 3).

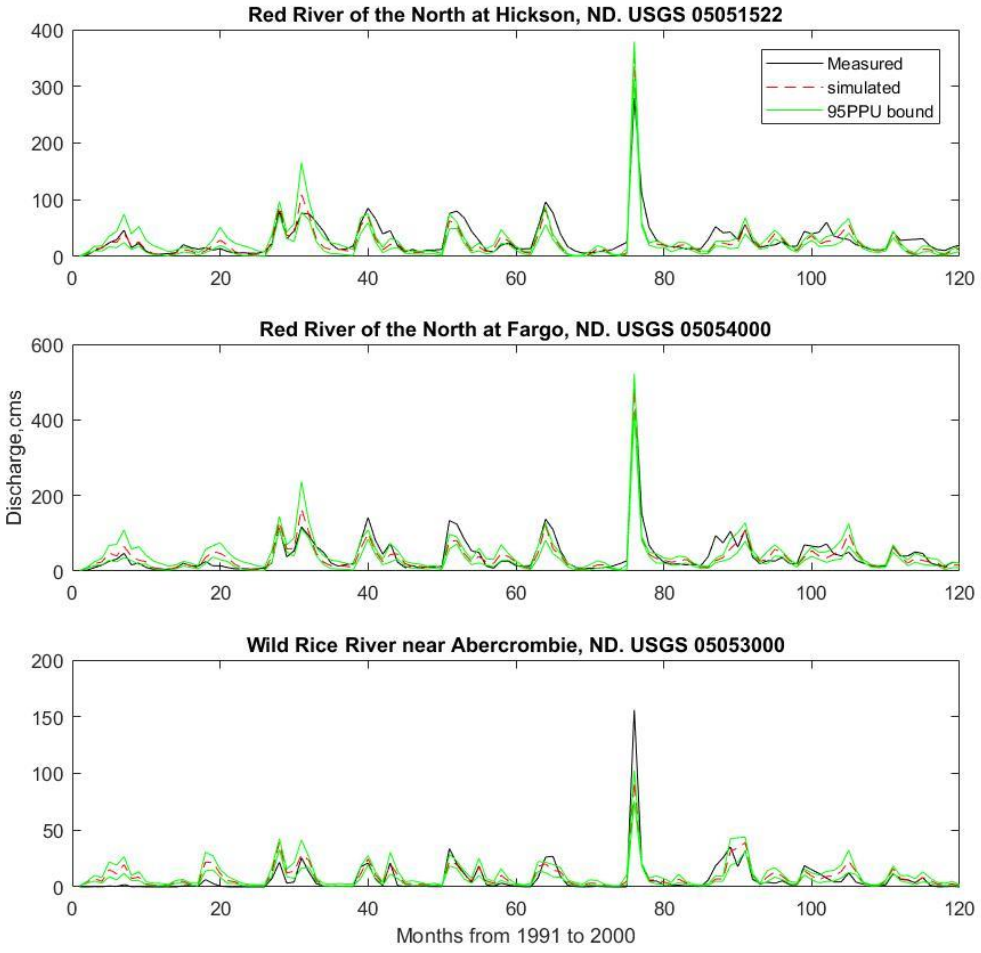

Figure 3. Measured versus simulated discharge during the model calibration period.

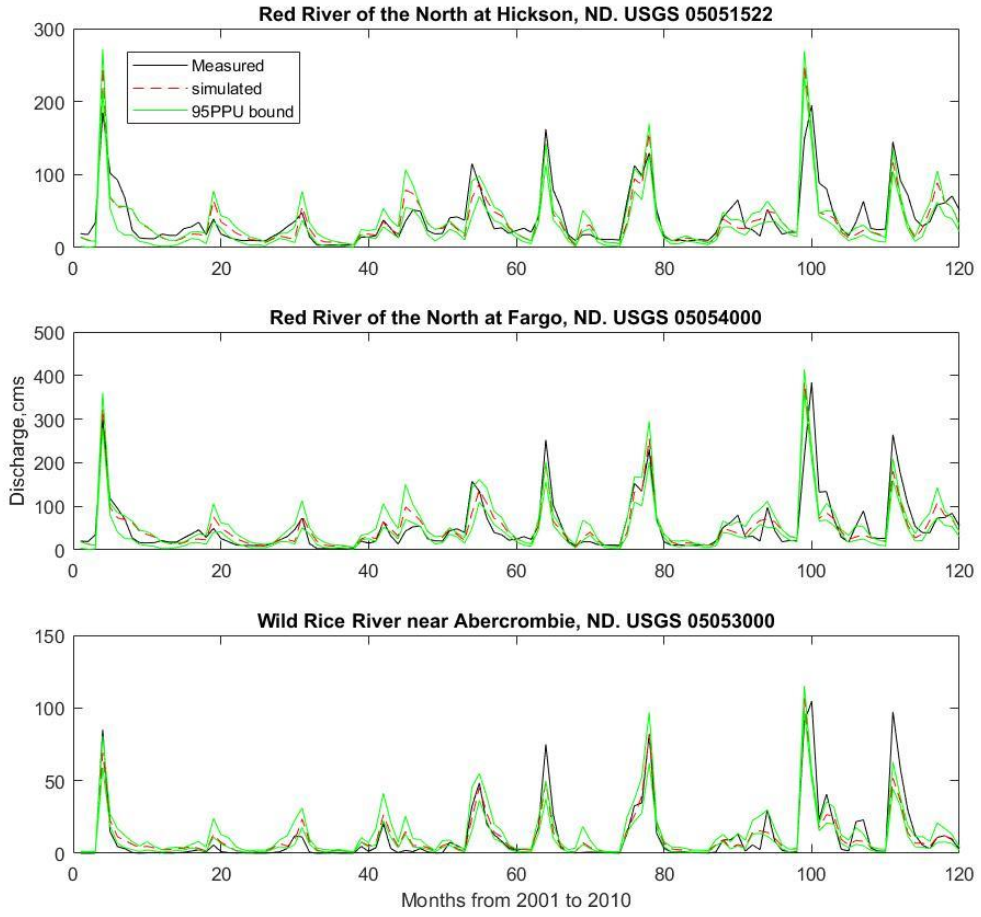

Figure 4. Measured versus simulated discharge during the model validation period.

Graphic comparison between the measured and simulated monthly average discharge indicates that for both the calibration and validation periods, the HAWQS output can generally predict the trend of streamflow in the study watershed and can also capture the period with extremely large discharge. However, a wider uncertainty band was observed for the months with relatively high discharge, as well as a narrower band for the low discharge months, indicating that the model has more accurate representation

for low streamflow during dry seasons, yet is less confident in predicting large discharge events during rainfall or snowmelt seasons (Figure 3 and Figure 4). The final results for the calibration and validation process are the range of parameters generated from the last calibration iteration, yet only the "best values" giving the optimal objective function value in the last iteration were used for the predictive simulations. The solution parameter ranges and the best parameter set, along with the corresponding method of change for each hydrological parameter, are documented in Table 4.

Table 4. Output hydrology parameters of calibration and validation periods.

Hydrology Parameter	Method of Change	Minimum Value	Maximum Value	Best Value
CN2	Relative	–0.02603	0.026317	0.000756
ALPHA_BF	Replace	0.442177	0.807037	0.537649
GWQMN	Absolute	–989.505	–426.971	–561.042
RCHRG_DP	Absolute	–0.00351	0.035731	0.003361
SFTMP	Replace	0.279737	0.894913	0.680627
SMFMX	Replace	4.029216	4.5	4.246561
SMFMN	Replace	0.885622	1.513742	1.447789
TIMP	Replace	0.517077	0.804303	0.518513
SOL_AWC	Relative	0.027779	0.047675	0.028011
ESCO	Replace	0.620969	0.781543	0.713834

2.6 Predictive Simulation Setup

2.6.1 Climate Change and General Circulation Models

Anthropogenic climate change induced by greenhouse effects has been widely discussed during recent decades; it is widely accepted that the increase in greenhouse gas, mainly CO_2, since the Industrial Revolution has incurred significant impact on the global climate pattern, and warming of the climate system is now evident based on the observed increase in global average surface temperature [*Solomon et al.*, 2007]. The 2007 Intergovernmental Panel on Climate Change (IPCC) report further pointed out that climate change is expected to have a more distinct impact on weather patterns in mid- and high-latitude regions in the northern hemisphere, and snowmelt and runoff in western North America has occurred at increasingly earlier times of a year since the late 1940s; some studies have even predicted that streamflow in colder climate zones is projected to change from the current snowmelt-driven, spring-flood-dominated flow regime to a dampened flow regime dominated by a large winter streamflow [*Parry et al.*, 2007; *Teutschbein and Seibert*, 2012].

The general circulation models (GCMs) are numerical models that simulate the impacts of increasing greenhouse gas concentration on the global climate system. The GCMs depict physical processes in the atmosphere using a three dimensional grid over the globe, which has a relatively coarse resolution that often cannot properly model physical processes on small local scales [*Parry et al.*, 2007]. One of the key uncertainties in climate projection is the uncertainty in future emissions, climate modelers apply several different emission scenarios to represent the emission related uncertainty. It is

pointed out in a previous study that the selection of climate scenarios in impact and adaptation assessments has often been arbitrary, and the selected scenarios rarely capture the entire range of uncertainties [*Ruosteenoja et al.*, 2003]. However, two future projection simulations with specified representative concentration pathways (RCPs), namely the high emission scenario (RCP8.5) and the midrange mitigation emission scenario (RCP4.5), are core set of scenarios that often conducted in the GCM experiments and used for long-term hydrological impact assessments [*Taylor et al.*, 2012].

Previous studies have used general circulation models on trends assessment of streamflow in North America, results of the studies generally indicate the rising global temperature could lead to increase of precipitation on the local scale [*Douglas et al.*, 2000]. Studies conducted by *Groisman and Easterling* [1994], and *Karl and Knight* [1998] also provide the similar prediction that precipitation amount and intensity across the US and Canada increased in the recent decades. More specifically on the region where the study area of this project is located, *Lettenmaier et al.* [1994] found strong increases in monthly streamflow during November through April from 1948 to 1988 in north central region of the United States, and an assessment of streamflow records from 36 USGS gage stations in Minnesota suggests that while the peak flow due to snowmelt does not appear to change at a significant rate, average discharge in the region have shown clear increase [*Novotny and Stefan*, 2007].

2.6.2 Description of Change Factor Methodology

Results from one of the general circulation models were applied as input climate signals for the predictive models in this project. Studies analyzing the hydrological response to the impacts of climate change are often conducted by coupling a regional climate model with a hydrological model. Transferring the changing signals from climate models to hydrological models requires an interface [*Andréasson et al.*, 2004]. Although more sophisticated methods are now available for climate signal transferring, a popular and straightforward approach is to apply change factor methodology (CFM). General procedures for applying CFM include three steps: (1) establishing a baseline climatology for the weather variables in a study area, (2) calculating changes of the weather variables for the study area obtained from a climate model, and (3) adding the changes to the baseline time series [*Arnell and Reynard*, 1996; *Diaz-Nieto and Wilby*, 2005].

Based on the number of change factors (CFs), the CFM can be categorized into single and multiple CFs. Values of the interested weather variables are calculated identically for single CFs, while multiple CFs provide more variability that enables approximation of more complex climate scenarios and are calculated separately for different magnitudes of the interested variables [*Akhtar et al.*, 2008; *Anandhi et al.*, 2011; *Hay et al.*, 2000]. Two types of mathematical formulations are used to apply CFM: (1) addictive CFM, where the arithmetic difference between current climate data and future climate prediction for a variable is obtained from a GCM grid location, and the difference is then added to observed local weather data to generate future weather

data and (2) multiplicative CFM, where the ratio between current and predicted simulations is multiplied with observed local data [*Anandhi et al.*, 2011].

This study applied the single CF procedure for climate change assessment; moreover, both additive and multiplicative approaches were used. The additive approach calculates temperature data, and the multiplicative approach is used for precipitation.

The first step of the single CF procedure calculates the mean values of GCM baseline and future climate variables and can be represented by Equations 4 and 5:

$$\overline{GCMb} = \sum_{i=1}^{Nb} GCMb_i/Nb \tag{4}$$

$$\overline{GCMf} = \sum_{i=1}^{Nb} GCMf_i/Nf \tag{5}$$

where $GCMb_i$ and $GCMf_i$ are the values of baseline and future scenarios, $\overline{GCMb}$ and $\overline{GCMf}$ are the mean values for the given period, and Nb and Nf stand for the number of data points for each variable [*Anandhi et al.*, 2011], which in this study represents a number of days.

The second step calculates the additive (CF_{add}) and multiplicative (CF_{mul}) CF using Equations 5 and 6:

$$CF_{add} = \overline{GCMf} - \overline{GCMb} \tag{6}$$

$$CF_{mul} = \overline{GCMf}/\overline{GCMb} \tag{7}$$

Step three obtains the future climate data by applying CF to the observed local data, which can be represented using Equations 8 and 9:

$$Lf_{add,i} = LOb_i + CF_{add} \quad (8)$$

$$Lf_{mul,i} = LOb_i * CF_{mul} \quad (9)$$

where $Lf_{add,i}$ and $Lf_{mul,i}$ are the values of future scenarios obtained from additive and multiplicative CFs and LOb_i is the observed local climate time series [*Anandhi et al.*, 2011].

2.6.3 Weather Input Setup

Results from one of the GCMs, the Geophysical Fluid Dynamics Laboratory's global coupled carbon-climate earth system model with vertical coordinates based on density (GFDL-ESM2G) [*Dunne et al.*, 2012], were used to calculate CF in this project. The GFDL-ESM2G is a part of the CMIP5, which is conducted by 20 modeling groups around the world to produce a new set of coordinated climate model experiments [*Sheffield et al.*, 2013]. Assessments conducted in previous studies have confirmed that GFDL-ESM2G output has achieved sufficient fidelity for meaningful perturbation studies [*Dunne et al.*, 2012; *Sillmann et al.*, 2013].

Climate data obtained from the GCMs are often downscaled for application at the local scale [*Wilby and Wigley*, 1997]. In this project, the 1-degree observed climate data and 1-degree bias-corrected GCM projections of the GFDL-ESM2G were obtained from the "Downscaled CMIP3 and CMIP5 Climate and Hydrology Projections" online archive (http://gdo-dcp.ucllnl.org). The archive enables its users to define a tributary area as the spatial extent for the requested climate data by entering longitude and latitude values of a watershed outlet. Daily observed and projected data of RCP4.5 and RCP8.5 scenarios

for the study area with calculated spatial mean were downloaded from the archive, observed data from 1980 to 1999 were used as the baseline, and projected data from 2026 to 2045 were used as the future scenario for CF calculation.

Monthly CFs were calculated using Equations 4 to 9. For the two projection scenarios (RCP4.5 and RCP8.5) being analyzed, two sets of CFs were calculated on divided periods, CF for 2026 to 2035 used observations from 1980 to 1989 as its baseline, and CF for 2036 to 2045 used observations from 1990 to 1999. CF for precipitation was calculated using the multiplicative approach, with its results presented as percentages (Table 5). While for the temperature data an additive approach was applied, CF for maximum and minimum daily temperature was calculated separately and averaged to obtain the overall CF for temperature (Table 6).

Table 5. Monthly CF for precipitation, in percentage.

Period	2026 to 2035			2036 to 2045		
Emission Scenario	Monthly Precipitation of Baseline Period (mm)	RCP4.5	RCP8.5	Monthly Precipitation of Baseline Period (mm)	RCP4.5	RCP8.5
Jan	16.265	0.26	–13.47	20.860	–9.04	–16.71
Feb	11.815	41.25	39.04	13.886	–37.25	–1.23
Mar	29.183	–13.34	59.15	30.941	8.28	–20.79
Apr	35.715	60.51	65.78	45.634	55.72	26.00
May	64.410	9.29	22.85	74.329	16.04	35.12
Jun	84.946	37.84	27.16	109.850	27.87	–2.99
Jul	83.018	5.07	14.97	102.674	1.43	–6.29
Aug	83.901	12.32	11.37	72.758	-5.65	10.97
Sep	61.977	41.87	28.89	62.184	6.54	4.01
Oct	50.253	5.37	–2.12	54.637	–28.79	–26.54
Nov	23.951	15.72	12.43	25.098	–9.78	–4.90
Dec	11.494	69.96	78.29	12.740	21.00	32.29

Table 6. Monthly CF for temperature, in degC.

Period	2026 to 2035			2036 to 2045		
Emission Scenario	Average Monthly Temperature of Baseline Period (degC)	RCP 4.5	RCP 8.5	Average Monthly Temperature of Baseline Period (degC)	RCP 4.5	RCP 8.5
Jan	–12.31	0.640	2.624	–13.36	1.925	2.002
Feb	–9.55	0.872	0.663	–8.59	0.315	0.790
Mar	–2.42	0.739	0.026	–2.67	2.205	0.948
Apr	7.25	0.486	0.312	5.58	0.892	1.538
May	14.44	–0.756	–1.296	13.55	0.364	–0.207
Jun	18.45	–0.175	0.453	18.76	–0.842	–0.189
Jul	22.08	–0.456	–0.089	20.13	0.570	1.759
Aug	20.28	0.104	1.971	20.15	0.822	1.512
Sep	13.98	1.287	1.969	14.90	0.597	3.011
Oct	7.06	1.816	2.575	7.41	2.330	2.601
Nov	–2.18	2.342	0.992	–2.69	1.550	2.654
Dec	–10.98	2.967	3.184	–8.86	1.565	0.784

Despite the fact that HAWQS possesses most of the functions and capabilities of SWAT and enables its users to edit commonly sensitive hydrological parameters, it still lacks the option to edit all existing parameters, a feature that SWAT has. In addition, the operations for conducting climate variability analysis are comparatively limited in HAWQS at the current stage. Thus, another SWAT model interface, SWAT-Editor, was used to set up the predictive simulations. SWAT-Editor is a standalone application for

editing parameters and the SWAT database; it can run SWAT models without the support of ArcGIS. SWAT-Editor requires the input of a SWAT parameter geodatabase and a SWAT project database [*Winchell and Srinivasan*, 2012].

In this study, daily simulations from 1980 to 1999 of the study area were conducted using HAWQS; the output project files from HAWQS, which contains the unique project database, were used as the input for SWAT-Editor. The fitted parameters from the calibration procedure were adjusted in SWAT-Editor, and the calculated CFs for each month (Tables 5 and 6) were integrated into the model by adjusting the correlated subbasin parameters (Table 7). Four climate change predictive simulations were set up and run after these procedures (i.e., RCP4.5 from 2026 to 2035, RCP8.5 from 2026 to 2035, RCP4.5 from 2036 to 2045, and RCP8.5 from 2036 to 2045).

Table 7. Adjusted climate variability parameters [*Arnold et al.*, 2012].

SWAT Input Parameter	File Extension	Description
RFINC (mon)	.sub	Rainfall adjustment (% change). Daily rainfall within the month is adjusted by the specified percentage.
TMPINC (mon)	.sub	Temperature adjustment (degC). Daily maximum and minimum temperatures within the month are raised or lowered by the specified amount.

2.6.4 Flood Diversion Channel Setup in SWAT-Editor

Among the hydrological structures planned in the final EIS for the F-M flood risk

management project, the flood diversion channel plays the most significant role in reducing the flood risk of the F-M urban area. The diversion channel of the Red River starts near Horace, North Dakota, and is designed to extend 30 miles northward on the west side of the F-M urban area; an outlet of the diversion channel would meet the Red River near Georgetown, Minnesota (Figure 9 in Appendix A) [*Minnesota Department of Natural Resources*, 2016].

In evaluating the flood reduction capability of the flood management project for the urban area, discharge downstream the Red River is not a major concern given the low population density of the downstream area, so this study focused on assessing the projected streamflow of the Red River's main channel at the F-M urban area. Point-source loadings were applied in SWAT-Editor to represent the diversion channel. The diversion channel is designed to receive at maximum 566.34 m^3/s (20,000 ft^3/s) of discharge; the control structure at the diversion channel inlet enables artificial control of actual discharge in the channel. Additionally, although it is not clear right now how the local authority will manage the amount of discharge in the diversion channel, it is mentioned in the final EIS that the diversion channel would only be put to use when discharge in the Red River main channel could induce flood risk [*Minnesota Department of Natural Resources*, 2016].

Therefore, this study used a few simplified procedures to represent the complex nature of the real scenario for the diversion channel. After conducting the climate change predictive simulations in SWAT-Editor, the daily output discharge data of the subbasin

at the F-M urban area were queried to find the days with discharge larger than 631.46 m^3/s (22,300 ft^3/s). The 631.46-m^3/s discharge corresponds to 11.16 m (36.6 ft) of stage height for the USGS gage at Fargo (USGS 05054000), which is stated in the EIS as the amount of discharge at which significant flood damage can occur (Table 13 in Appendix A). The daily point-source files for each period and emission scenario were created based on the query conducted on the discharge output of the climate change predictive simulations, in which all the days with larger than 631.46-m^3/s discharge are applied with a daily total water extraction of 48,931,511.62 m^3, which matches the maximum diversion capability of 566.34 m^3/s.

CHAPTER III

RESULTS AND DISCUSSION

3.1 Results

Figure 5 shows the simulated and measured daily streamflow of the Red River at Fargo between 1980 and 1999, which is further divided into two periods, each with a decade-long record. Local weather input of these two periods was used as the baseline of the predictive simulations and was added or multiplied with the single CFs. Graphic comparison of the measured and simulated time series shows that model-simulated data on a daily time step generally capture the trend of observed streamflow; however, the comparison generally suggests overestimation for the entire modeling period.

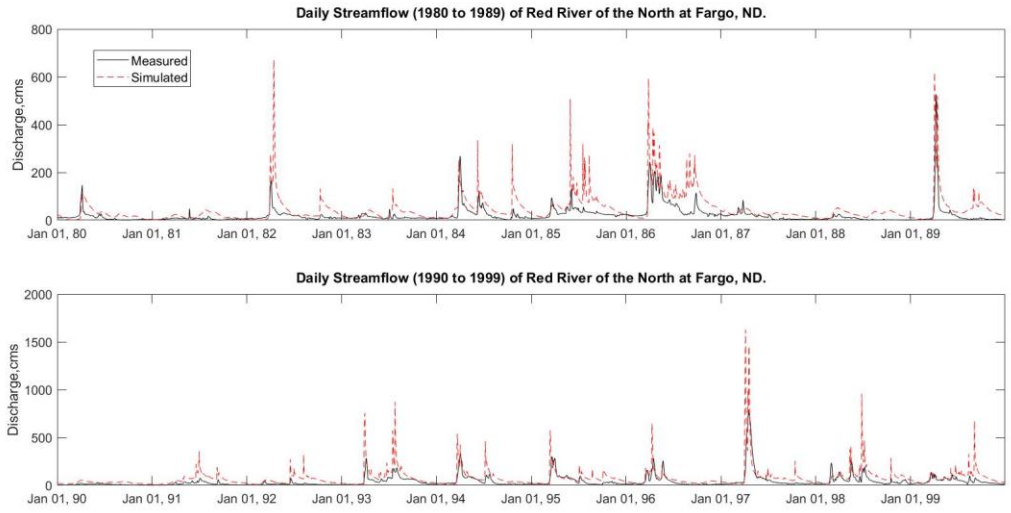

Figure 5. Two periods (1980 to 1989 and 1990 to 1999) of simulated and measured discharge of the Red River of the North at Fargo, ND.

Figure 6 and Figure 7 present the projected streamflow for 2026 to 2035 and 2036 to 2045. Four projected scenarios are included in each figure: the RCP4.5 and RCP8.5 without the flood diversion channel indicate future projections under the two emission scenarios without considering the effects of the flood management project, while the RCP4.5 and RCP8.5 with the diversion channel indicate the results when the diversion channel is included in the simulations in the form of point-source extraction. Graphic comparisons between the time series in Figure 6 and Figure 7 generally show that the diversion channel is effective at reducing the extremely large discharges of the Red River at Fargo. Furthermore, although not directly discernable from the figures, for the diversion-channel-included time series, daily discharge for the days without direct water extraction also sees a slight decrease.

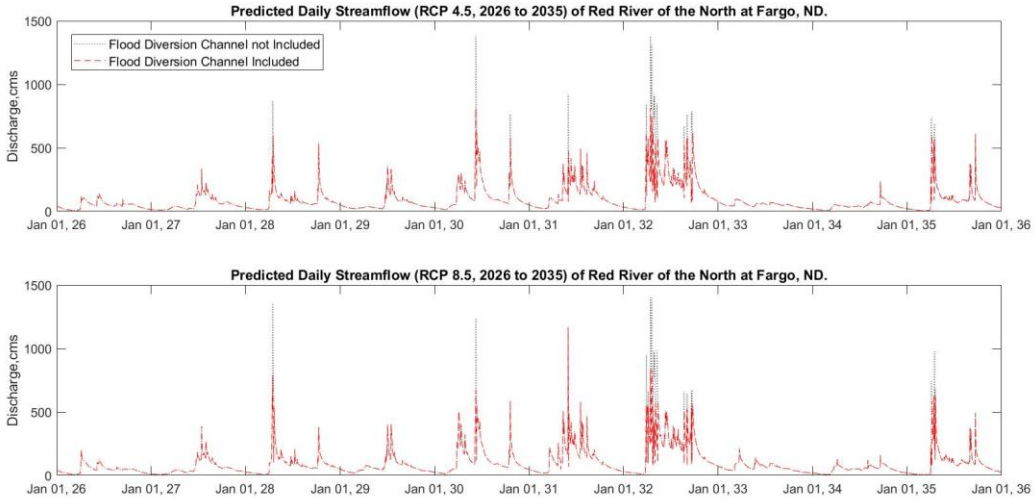

Figure 6. Predicted Daily Streamflow of the Red River at Fargo from 2026 to 2035 under four possible scenarios (RCP4.5 with diversion channel, RCP4.5 without diversion channel, RCP8.5 with diversion channel, RCP8.5 without diversion channel).

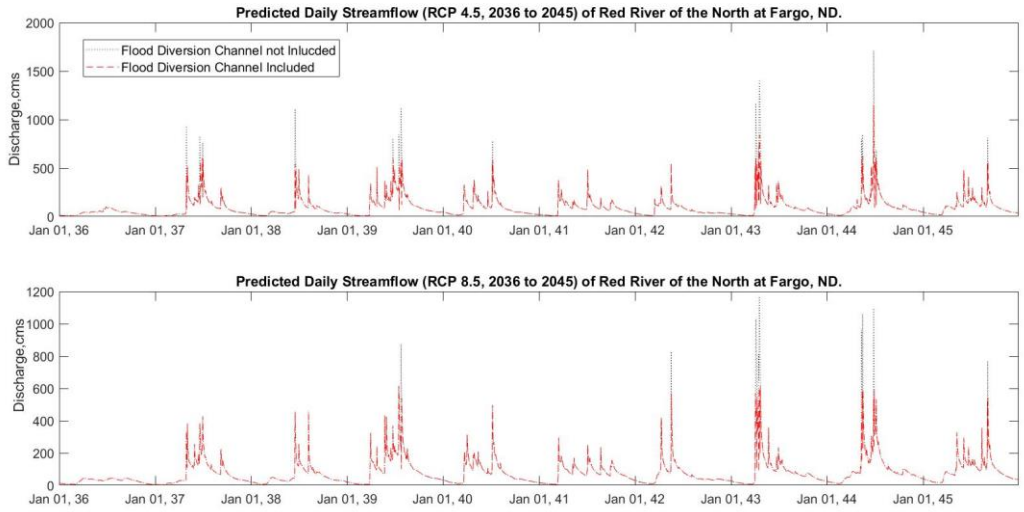

Figure 7. Predicted Daily Streamflow of the Red River at Fargo from 2036 to 2045 under four possible scenarios (RCP4.5 with diversion channel, RCP4.5 without diversion channel, RCP8.5 with diversion channel, RCP8.5 without diversion channel).

Statistics of the projected time series were calculated to investigate the variability of simulated streamflow. For the discharge of each projected scenario, mean, variance, coefficient of variation (CV, the standard deviation divided by the mean), and skewness were calculated. The CV accounts for the changes in streamflow variability associated with changes in the mean, whereas a positive skewness indicates a tendency of lower-streamflow days outnumbering higher-streamflow days [*Pagano and Garen*, 2005].

Table 8. Statistical results of the baseline and projected daily streamflow scenarios for 2026 to 2035 and 2036 to 2045, units in m^3/s.

Period			2026 to 2035		
Scenario	Baseline Scenario (1980-1989)	RCP4.5 Without Flood Diversion	RCP8.5 Without Flood Diversion	RCP4.5 With Flood Diversion	RCP8.5 With Flood Diversion
Mean	44.87	95.75	101.82	88.90	93.85
Variance	3343.07	15657.89	18149.37	9362.16	10357.35
Coefficient of Variation	1.29	1.31	1.32	1.09	1.08
Skewness	4.16	4.03	4.12	2.69	2.76
Period			2036 to 2045		
Scenario	Baseline Scenario (1990-1999)	RCP4.5 Without Flood Diversion	RCP8.5 Without Flood Diversion	RCP4.5 With Flood Diversion	RCP8.5 With Flood Diversion
Mean	73.97	96.81	80.13	90.73	76.85
Variance	9730.80	15413.55	9591.17	9208.27	6230.34
Coefficient of Variation	1.33	1.28	1.22	1.06	1.03
Skewness	6.80	4.48	4.62	2.80	2.66

The statistical results (Table 8) generally demonstrate that, overall, the projected streamflow under each period and emission scenario is wetter than the corresponding

baseline scenario. More specifically, the RCP8.5 scenarios are wetter (higher mean) from 2026 to 2035, but drier (lower mean) in the following decade compared with RCP4.5 scenarios. Furthermore, the drier period has always been associated with lower-streamflow variability (lower mean corresponds with lower variance and CV). Lower variance and CV were observed for the scenarios that include the diversion channel, indicating that the flood diversion project can significantly reduce the streamflow variability of the Red River at Fargo. Positive skewness was observed for all the projected streamflow scenarios, suggesting that the flow regime of the Red River would still be dominated by relatively low-streamflow days for the majority of the simulation time; however, a few extremely large discharge predictions will heavily influence the shape of the time series distribution.

To further assess the effectiveness of the F-M flood diversion project, the number of days for different magnitudes of flood recurrence intervals of the Red River at Fargo was queried from the simulation output of each scenario. The original discharge threshold data for each magnitude of recurrence intervals (Table 9) were obtained from the Federal Emergency Management Agency (FEMA) Clay County Flood Insurance Study and were documented in the final EIS for the F-M flood risk management project [*Minnesota Department of Natural Resources*, 2016]. Results of the query are displayed in Figure 8. For the decade between 2026 and 2035, RCP8.5 scenarios predict more flood events than RCP4.5 scenarios, whereas the situation reverses for the following decade. In the predictive simulations, the diversion channel is only added into the model when discharge exceeds 631.46 m^3/s (22,300 ft^3/s; i.e., 50-year FEMA), the number of

flood events with high magnitude (i.e., 50-, 100-, and 500-year FEMA) is significantly reduced when the diversion channel is included; however, the number of low-magnitude flood events (i.e., 10-year FEMA) slightly increases (Figure 8 and Table 14 in Appendix A).

More specifically, the predictive simulations indicate that extracting water through the diversion channel during high-flow days completely eliminates occurrence of a 500-year flood and eliminates occurrence of a 100-year flood under drier projections (i.e., RCP4.5 from 2026 to 2035, RCP8.5 from 2036 to 2045), whereas under wetter projections, an 88% reduction in 100-year flood events is predicted under scenario RCP8.5 from 2026 to 2035, with three daily flow events exceeding the 100-year recurrence interval predicted to occur. An 88.89% reduction of 100-year flood events is predicted under scenario RCP8.5 from 2036 to 2045, with another two daily flow projections exceeding the 100-year recurrence interval. The 50-year flood is eliminated under RCP8.5 scenarios from 2036 to 2045, whereas for the other three predictive scenarios, the number of 50-year floods is reduced by around 85%. The number of occurrences for the 10-year flood sees a slight increase ranging from 6.83% to 10.84% (Table 10).

Table 9. FEMA Peak flow and stage data of USGS gage at Fargo, data obtained from Clay County Flood Insurance Study [*Minnesota Department of Natural Resources*, 2016].

Event	Discharge (ft^3/s)	Stage (ft)	Discharge (m^3/s)	Stage (m)
10-year FEMA	10,300	29.5	291.66	9.0
50-year FEMA	22,300	36.6	631.46	11.2
100-year FEMA	29,300	39.3	829.68	12.0
500-year FEMA	50,000	43.5	1415.83	13.3

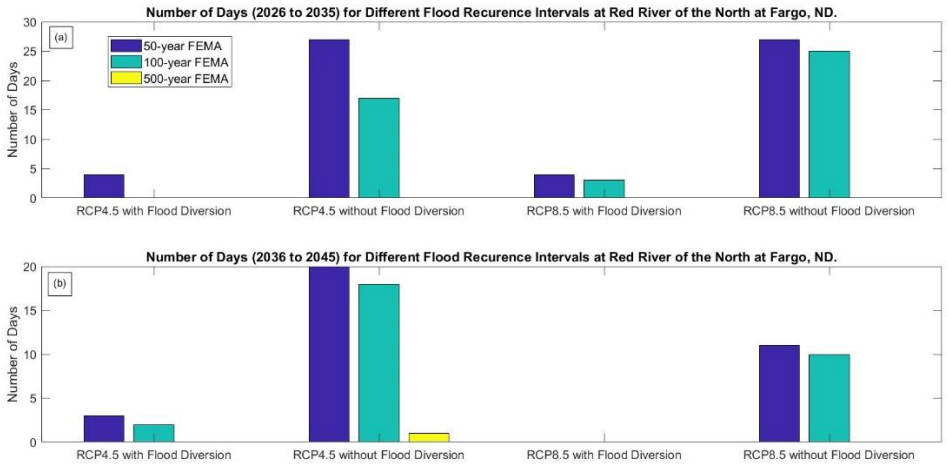

Figure 8. The number of days from (a) 2026 to 2035 and (b) 2036 to 2045 with 10-, 50-, 100-, and 500-year flood magnitudes under four projected discharge scenarios (RCP4.5 with flood diversion, RCP4.5 without flood diversion, RCP8.5 with flood diversion, and RCP8.5 without flood diversion).

Table 10. Percent change of the number of different-magnitude flood events when diversion channel is included.

Period	2026 to 2035		2036 to 2045	
Scenario	RCP4.5	RCP8.5	RCP4.5	RCP8.5
50-year	–85.19	–85.19	–85.00	–100.00
100-year	–100.00	–88.00	–88.89	–100.00
500-year	NA	NA	–100.00	NA

3.2 Discussion

The streamflow output from projected climate change scenarios shows that from 2026 to 2035, the RCP4.5 emission scenario predicts a wetter condition for the study area compared with the RCP8.5 scenario, whereas from 2036 to 2045, the RCP4.5 scenario predicts a drier condition. The diversion channel on the west side of Fargo is the most important structural measure of the F-M flood management project and is simplified as a point source, which is added into the model using SWAT-Editor. The diversion channel is only included on selected days with fairly large discharge; output of the model scenarios with water extraction in this manner indicates that the diversion channel is effective at reducing the number of large-magnitude streamflow events (50-, 100-, and 500-year recurrence intervals).

While assessing the results of simulations, it is important to point out that some limitations in the methodology can induce potential errors for the predictions of this study. Given the relatively large number of subbasins created in the HAWQS for the

study area and limited computational resources, the HAWQS was calibrated in a monthly time step, and the calibrated parameters were transferred temporally to produce daily predictions for future scenarios. As shown in Figure 5 where the simulated daily streamflow generally overestimates the observed data, the error can be transmitted into the predictive simulations and can cause overestimation of future floods.

In addition, the structural measures of the F-M flood management project were oversimplified in the predictive simulation designs in this study. Although the flood diversion channel was included in the analysis, other structure measures, such as additional embankments and staging area for flood storage were not incorporated into the evaluation. Moreover, the approach of simulating the diversion channel in this study is to only apply water extraction on days with discharge exceeding the 50-year recurrence interval, whereas in a practical situation, the amount of water diverted from the Red River can be artificially manipulated through the inlet control structure, thereby creating much more complex scenarios of flood diversion than the model simulations.

The approach for incorporating future climate variation can introduce error to the output as well. In this study, results from only one GCM were used for the calculation of CFs. Future analysis on this topic can use more GCMs to generate scenarios for comparison purposes. Another limitation associated with weather input is a common disadvantage of applying single CFM, in which the temporal sequencing of wet and dry days generally remains unchanged between baseline simulation and predictive simulation [*Anandhi et al.*, 2011]. In this study, the predictive daily time series (Figure 6

and Figure 7) also followed the temporal sequence of the baseline time series from 1980 to 1999 (Figure 5).

CHAPTER IV

SUMMARY AND CONCLUSIONS

The objective of this study was to analyze the streamflow regime variation of the Red River of the North at Fargo under different future climate projections and to evaluate the effectiveness of the F-M flood diversion project in reducing the magnitude of potential flood events. The upper Red River basin was selected as the study watershed, with its outlet overlay within the F-M urban area. HAWQS was used to set up the hydrologic simulations for the study area, and a simulation with a monthly time step was performed for sensitivity analysis, model calibration, and model validation, which were conducted using the SWAT-CUP SUFI2 procedure. After the calibration process, HAWQS was used to set up a new simulation with a daily time step. The daily simulation project database generated using HAWQS was connected to SWAT-Editor, in which the calibrated parameter and the future climate projections from a GCM were edited. Predictive simulations were set up under RCP4.5 and RCP8.5 emission scenarios for two separate periods, 2026 to 2035 and 2036 to 2045, which represent the short- to medium-terms following completion of the flood diversion project. After setting up the climate change scenarios, the diversion channel was added to each scenario in the form of point-source water extraction.

Results from this study show that the Red River of the North would experience wetter conditions under all projected climate change scenarios for the entire time span of the predictive simulations. Meanwhile, the implementation of the diversion channel near

the F-M urban area would have a significant impact on the flow regime of the Red River in this area, and a streamflow pattern with lower average discharge and lower flow variability is predicted for the simulations when flood diversion is included. The effectiveness of the flood diversion channel was further evaluated by querying the number of days of different-magnitude flood events for each predictive scenario. Results of the query show a clear reduction in large-magnitude events.

Some important limitations of this study include the model calibration and validation being performed on a monthly time step and the predictive simulations being performed on a daily time step, as well as the procedure of transferring parameters through a temporal scale potentially leading to errors in the predictive model. In the future climate projections produced from single CFM, the temporal sequencing of wet and dry days in the predictive simulations generally remains unchanged. In addition, the oversimplification of the flood diversion channel in the model simulations cannot realistically represent the complex situation when the flood diversion project is put into actual use. For future works on this topic, it is preferable to have the calibration and validation process performed on a daily time step. Moreover, results from more GCMs could be incorporated to create additional predictive scenarios for verification purposes, and the time span for the predictive simulations could be extended to a longer period in order to achieve more thorough evaluation for the F-M flood diversion project.

REFERENCES

Abbaspour, K. C. (2011), SWAT-CUP4: SWAT calibration and uncertainty programs–a user manual, Swiss Federal Institute of Aquatic Science and Technology, Eawag.

Abbaspour, K., E. Rouholahnejad, S. Vaghefi, R. Srinivasan, H. Yang, and B. Kløve (2015), A continental-scale hydrology and water quality model for Europe: Calibration and uncertainty of a high-resolution large-scale SWAT model, Journal of Hydrology, 524, 733-752.

Abbaspour, K., J. Yang, I. Maximov, R. Siber, K. Bogner, J. Mieleitner, J. Zobrist, and R. Srinivasan (2006), Modelling hydrology and water quality in the pre-alpine/alpine Thur watershed using SWAT, Journal of Hydrology, 333, 2-4.

Abbaspour, K. C., M. Faramarzi, S. S. Ghasemi, and H. Yang (2009), Assessing the impact of climate change on water resources in Iran, Water resources research, 45(10).

Akhtar, M., N. Ahmad, and M. J. Booij (2008), The impact of climate change on the water resources of Hindukush–Karakorum–Himalaya region under different glacier coverage scenarios, Journal of Hydrology, 355(1-4), 148-163.

Anandhi, A., A. Frei, D. C. Pierson, E. M. Schneiderman, M. S. Zion, D. Lounsbury, and A. H. Matonse (2011), Examination of change factor methodologies for climate change impact assessment, Water Resources Research, 47(3).

Andréasson, J., S. Bergström, B. Carlsson, L. P. Graham, and G. Lindström (2004), Hydrological change–climate change impact simulations for Sweden, AMBIO: A Journal of the Human Environment, 33(4), 228-234.

Arnell, N., and N. Reynard (1996), The effects of climate change due to global warming on river flows in Great Britain, Journal of hydrology, 183(3-4), 397-424.

Arnold, J., J. Kiniry, R. Srinivasan, J. Williams, S. Haney, and S. Neitsch (2012), Soil and Water Assessment Tool Input/Output Documentation, Version 2012, Texas Water Resources Institute, Temple, TX, USA*Rep.*, TR-439.

Barrett, J. P. (1974), The coefficient of determination—some limitations, The American Statistician, 28(1), 19-20.

Cao, W., W. B. Bowden, T. Davie, and A. Fenemor (2006), Multi‐variable and multi‐site calibration and validation of SWAT in a large mountainous catchment with high spatial variability, Hydrological Processes, 20(5), 1057-1073.

Chu, T., and A. Shirmohammadi (2004), Evaluation of the SWAT model's hydrology component in the piedmont physiographic region of Maryland, Transactions of the ASAE, 47(4), 1057.

Daggupati, P., H. Yen, M. J. White, R. Srinivasan, J. G. Arnold, C. S. Keitzer, and S. P. Sowa (2015), Impact of model development, calibration and validation decisions on hydrological simulations in West Lake Erie Basin, Hydrological Processes, 29(26), 5307-5320.

Diaz-Nieto, J., and R. L. Wilby (2005), A comparison of statistical downscaling and climate change factor methods: impacts on low flows in the River Thames, United Kingdom, Climatic Change, 69(2), 245-268.

Douglas, E., R. Vogel, and C. Kroll (2000), Trends in floods and low flows in the United States: impact of spatial correlation, Journal of Hydrology, 240(1), 90-105.

Dunne, J. P., J. G. John, A. J. Adcroft, S. M. Griffies, R. W. Hallberg, E. Shevliakova, R. J. Stouffer, W. Cooke, K. A. Dunne, and M. J. Harrison (2012), GFDL's ESM2 global coupled climate–carbon earth system models. Part I: Physical formulation and baseline simulation characteristics, Journal of Climate, 25(19), 6646-6665.

Dutta, D., S. Herath, and K. Musiake (2006), An application of a flood risk analysis system for impact analysis of a flood control plan in a river basin, Hydrological Processes, 20(6), 1365-1384, doi: 10.1002/hyp.6092.

Fant, C., R. Srinivasan, B. Boehlert, L. Rennels, S. C. Chapra, K. M. Strzepek, J. Corona, A. Allen, and J. Martinich (2017), Climate Change Impacts on US Water Quality Using Two Models: HAWQS and US Basins, Water, 9(2), 118.

Feyereisen, G., T. Strickland, D. Bosch, and D. Sullivan (2007), Evaluation of SWAT manual calibration and input parameter sensitivity in the Little River watershed, Transactions of the ASABE, 50(3), 843-855.

Ficklin, D. L., and B. L. Barnhart (2014), SWAT hydrologic model parameter uncertainty and its implications for hydroclimatic projections in snowmelt-dependent watersheds, Journal of Hydrology, 519, 2081-2090.

Fontaine, T., T. Cruickshank, J. Arnold, and R. Hotchkiss (2002), Development of a snowfall–snowmelt routine for mountainous terrain for the soil water assessment tool (SWAT), Journal of Hydrology, 262(1), 209-223.

Gassman, P. W., M. R. Reyes, C. H. Green, and J. G. Arnold (2007), The soil and water assessment tool: historical development, applications, and future research directions, Transactions of the ASABE, 50(4), 1211-1250.

Groisman, P. Y., and D. R. Easterling (1994), Variability and trends of total precipitation and snowfall over the United States and Canada, Journal of Climate, 7(1), 184-205.

Gupta, H. V., S. Sorooshian, and P. O. Yapo (1999), Status of automatic calibration for hydrologic models: Comparison with multilevel expert calibration, Journal of Hydrologic Engineering, 4(2), 135-143.

Harmel, R., P. Smith, K. Migliaccio, I. Chaubey, K. Douglas-Mankin, B. Benham, S. Shukla, R. Muñoz-Carpena, and B. J. Robson (2014), Evaluating, interpreting, and communicating performance of hydrologic/water quality models considering intended use: A review and recommendations, Environmental modelling & software, 57, 40-51.

Harmel, R. D., and P. K. Smith (2007), Consideration of measurement uncertainty in the evaluation of goodness-of-fit in hydrologic and water quality modeling, Journal of Hydrology, 337(3), 326-336.

Hay, L. E., R. L. Wilby, and G. H. Leavesley (2000), A comparison of delta change and downscaled GCM scenarios for three mountainous basins in the United States, JAWRA Journal of the American Water Resources Association, 36(2), 387-397.

Hearne, R. R. (2007), Evolving water management institutions in the Red River Basin, Environ Manage, 40(6), 842-852, doi: 10.1007/s00267-007-9026-x.

Jayakrishnan, R., R. Srinivasan, C. Santhi, and J. Arnold (2005), Advances in the application of the SWAT model for water resources management, Hydrological processes, 19(3), 749-762.

Karl, T. R., and R. W. Knight (1998), Secular trends of precipitation amount, frequency, and intensity in the United States, Bulletin of the American Meteorological society, 79(2), 231-241.

Lee, T., R. Srinivasan, J. Moon, and N. Omani (2011), Estimation of fresh water inflow to bays from gaged and ungaged watersheds, Applied engineering in agriculture, 27(6), 917-923.

Lenhart, T., K. Eckhardt, N. Fohrer, and H.-G. Frede (2002), Comparison of two different approaches of sensitivity analysis, Physics and Chemistry of the Earth, Parts A/B/C, 27(9), 645-654.

Licciardello, F., C. Rossi, R. Srinivasan, S. Zimbone, and S. Barbagallo (2011), Hydrologic evaluation of a Mediterranean watershed using the SWAT model with multiple PET estimation methods, Transactions of the ASABE, 54(5), 1615-1625.

Messner, F., and V. Meyer (2006), Flood damage, vulnerability and risk perception–challenges for flood damage research, Flood risk management: hazards, vulnerability and mitigation measures, 149-167.

Miller, J. E., and D. L. Frink (1984), Changes in flood response of the Red River of the North basin, North Dakota-Minnesota*Rep.*, United States Government Printing Office.

Minnesota Department of Natural Resources (2016), Final Environmental Impact Statement Fargo-Moorhead Flood Risk Management Project, edited by Minnesota Department of Natural Resources, St. Paul, MN.

Moriasi, D. N., J. G. Arnold, M. W. Van Liew, R. L. Bingner, R. D. Harmel, and T. L. Veith (2007), Model evaluation guidelines for systematic quantification of accuracy in watershed simulations, Transactions of the ASABE, 50(3), 885-900.

Nash, J. E., and J. V. Sutcliffe (1970), River flow forecasting through conceptual models part I—A discussion of principles, Journal of Hydrology, 10(3), 282-290.

Neitsch, S. L., J. G. Arnold, J. R. Kiniry, and J. R. Williams (2011), Soil and water assessment tool theoretical documentation version 2009*Rep.*, Texas Water Resources Institute.

Novotny, E. V., and H. G. Stefan (2007), Stream flow in Minnesota: indicator of climate change, Journal of Hydrology, 334(3), 319-333.

Olivera, F., M. Valenzuela, R. Srinivasan, J. Choi, H. Cho, S. Koka, and A. Agrawal (2006), ArcGIS‐SWAT: A geodata model and GIS interface for SWAT, JAWRA Journal of the American Water Resources Association, 42(2), 295-309.

Omani, N., R. Srinivasan, R. Karthikeyan, V. Reddy, and P. K. Smith (2016), Impacts of climate change on the glacier melt runoff from five river basins.

Pagano, T., and D. Garen (2005), A recent increase in western US streamflow variability and persistence, Journal of Hydrometeorology, 6(2), 173-179.

Parry, M. L., O. F. Canziani, J. P. Palutikof, P. J. van der Linden, and C. E. Hanson (2007), IPCC, 2007: climate change 2007: impacts, adaptation and vulnerability. Contribution of working group II to the fourth assessment report of the intergovernmental panel on climate change, edited, Cambridge University Press, Cambridge.

Peterson, J., and J. Hamlett (1998), Hydrologic calibration of the SWAT model in a watershed containing fragipan soils, JAWRA Journal of the American Water Resources Association, 34(3), 531-544.

Plate, E. J. (2002), Flood risk and flood management, Journal of Hydrology, 267(1), 2-11.

Qi, C., and S. Grunwald (2005), GIS-based hydrologic modeling in the Sandusky watershed using SWAT, Transactions of the ASAE, 48(1), 169-180.

Rouholahnejad, E., K. C. Abbaspour, M. Vejdani, R. Srinivasan, R. Schulin, and A. Lehmann (2012), A parallelization framework for calibration of hydrological models, Environmental Modelling & Software, 31, 28-36.

Ruosteenoja, K., T. R. Carter, K. Jylhä, and H. Tuomenvirta (2003), Future climate in world regions: an intercomparison of model-based projections for the new IPCC emissions scenarios.

Schuol, J., K. C. Abbaspour, R. Srinivasan, and H. Yang (2008a), Estimation of freshwater availability in the West African sub-continent using the SWAT hydrologic model, Journal of hydrology, 352(1), 30-49.

Schuol, J., K. C. Abbaspour, H. Yang, R. Srinivasan, and A. J. Zehnder (2008b), Modeling blue and green water availability in Africa, Water Resources Research, 44(7).

Sheffield, J., A. P. Barrett, B. Colle, D. Nelun Fernando, R. Fu, K. L. Geil, Q. Hu, J. Kinter, S. Kumar, and B. Langenbrunner (2013), North American climate in CMIP5 experiments. Part I: evaluation of historical simulations of continental and regional climatology, Journal of Climate, 26(23), 9209-9245.

Sillmann, J., V. Kharin, X. Zhang, F. Zwiers, and D. Bronaugh (2013), Climate extremes indices in the CMIP5 multimodel ensemble: Part 1. Model evaluation in the present climate, Journal of Geophysical Research: Atmospheres, 118(4), 1716-1733.

Solomon, S., D. Qin, M. Manning, Z. Chen, M. Marquis, K. Averyt, M. Tignor, and H. Miller (2007), IPCC, 2007: summary for policymakers, Climate change, 2007, 79.

Spatial Sciences Laboratory Texas A&M AgriLife Research (2016), HAWQS User Guide, edited by Spatial Sciences Laboratory, College Station, TX.

Srinivasan, R., and J. G. Arnold (1994), Integration of a basin‐scale water quality model with GIS, JAWRA Journal of the American Water Resources Association, 30(3), 453-462.

Stewart, I. T., D. R. Cayan, and M. D. Dettinger (2005), Changes toward earlier streamflow timing across western North America, Journal of Climate, 18(8), 1136-1155.

Stoner, J. D., D. L. Lorenz, G. J. Wiche, and R. M. Goldstein (1993), Red River of the North Basin, Minnesota, North Dakota, and South Dakota, JAWRA Journal of the American Water Resources Association, 29(4), 575-615.

Taylor, K. E., R. J. Stouffer, and G. A. Meehl (2012), An overview of CMIP5 and the experiment design, Bulletin of the American Meteorological Society, 93(4), 485-498.

Teutschbein, C., and J. Seibert (2012), Bias correction of regional climate model simulations for hydrological climate-change impact studies: Review and evaluation of different methods, Journal of Hydrology, 456, 12-29.

Tuppad, P., K. Douglas-Mankin, T. Lee, R. Srinivasan, and J. Arnold (2011), Soil and Water Assessment Tool (SWAT) hydrologic/water quality model: Extended capability and wider adoption, Transactions of the ASABE, 54(5), 1677-1684.

U.S. Army Corps of Engineers (2011), Final Feasibility Report and Environmental Impact Statement Fargo-Moorhead Metropolitan Area Flood Risk Management, edited by U.S. Army Corps of Engineers, St. Paul, MN.

Wang, X., and A. Melesse (2005), Evaluation of the SWAT model's snowmelt hydrology in a northwestern Minnesota watershed, Transactions of the ASAE, 48(4), 1359-1376.

Wilby, R. L., and T. Wigley (1997), Downscaling general circulation model output: a review of methods and limitations, Progress in physical geography, 21(4), 530-548.

Winchell, M., and R. Srinivasan (2012), SWAT Editor for SWAT 2012 Documentation*Rep.*, Blackland Research Center, Texas Agricultural Experiment Station. Grassland, Soil and Water Research Laboratory, USDA Agricultural Research Service.

Yang, J., P. Reichert, K. Abbaspour, J. Xia, and H. Yang (2008), Comparing uncertainty analysis techniques for a SWAT application to the Chaohe Basin in China, Journal of Hydrology, 358(1), 1-23.

Yen, H., P. Daggupati, M. J. White, R. Srinivasan, A. Gossel, D. Wells, and J. G. Arnold (2016), Application of large-scale, multi-resolution watershed modeling framework using the Hydrologic and Water Quality System (HAWQS), Water, 8(4), 164.

Zhang, X., R. Srinivasan, and M. Van Liew (2008), Multi-site calibration of the SWAT model for hydrologic modeling, Transactions of the ASABE, 51(6), 2039-2049.

Zhang, X., R. Srinivasan, and M. V. Liew (2010), On the use of multi‐algorithm, genetically adaptive multi‐objective method for multi‐site calibration of the SWAT model, Hydrological Processes, 24(8), 955-969.

Zhang, X., R. Srinivasan, K. Zhao, and M. V. Liew (2009), Evaluation of global optimization algorithms for parameter calibration of a computationally intensive hydrologic model, Hydrological Processes, 23(3), 430-441.

APPENDIX A

Table 11. Land use distribution of the study watershed.

Land Use	Area	% of Total Area	Description
SOYC	3,351.80 km2	19.7	Soybean-Corn rotation
CSOY	3,213.07 km2	18.88	Corn-Soybean rotation
FRSD	1,789.63 km2	10.52	Forest-Deciduous
WATR	1,394.10 km2	8.19	Water
SOYB	1,099.00 km2	6.46	Soybean
CORN	1,010.31 km2	5.94	Corn
WETN	953.00 km2	5.6	Wetlands-Nonforested
URLD	652.37 km2	3.83	Residential-Low Density
RNGE	848.90 km2	4.99	Range-Grasses
HAY	894.74 km2	5.26	Hay
SYSW	766.54 km2	4.5	Soybean-Spring Wheat rotation
SWSY	448.99 km2	2.64	Spring Wheat-Soybean rotation
SWHT	329.36 km2	1.94	Spring Wheat
SWCR	14.35 km2	0.08	Spring Wheat-Corn rotation
ALFA	87.91 km2	0.52	Alfalfa
URMD	67.43 km2	0.4	Residential-Medium Density
WETF	19.72 km2	0.12	Wetlands-Forested
FRSE	22.74 km2	0.13	Forest-Evergreen

Table 11. Continued.

Land Use	Area	% of Total Area	Description
URHD	30.34 km2	0.18	Residential-High Density
RNGB	10.39 km2	0.06	Range-Brush
CRSW	-	-	Corn-Spring Wheat rotation
UIDU	11.25 km2	0.07	Industrial
SWRN	-	-	Southwestern US (Arid) Range
WWHT	-	-	Winter Wheat
SFSW	-	-	Sunflower-Spring Wheat rotation
SWSF	-	-	Spring Wheat-Sunflower rotation
FRST	-	-	Forest-Mixed
SWCA	-	-	Spring Wheat-Canola rotation

Table 12. T-test results for the sensitivity analysis.

Parameter Name	t-Stat	P-Value
9:V__SMTMP.bsn	0.04	0.97
6:A__REVAPMN.gw	0.08	0.94
3:A__GW_DELAY.gw	0.26	0.80
5:V__GW_REVAP.gw	–0.34	0.75
12:V__TIMP.bsn	–0.54	0.61
2:V__ALPHA_BF.gw	0.89	0.42
10:V__SMFMX.bsn	–0.89	0.41
8:V__SFTMP.bsn	1.06	0.34
14:V__ESCO.hru	1.54	0.18
4:A__GWQMN.gw	–1.55	0.18
7:A__RCHRG_DP.gw	–1.59	0.17
13:R__SOL_AWC(..).sol	–1.78	0.13
11:V__SMFMN.bsn	2.06	0.09
1:R__CN2.mgt	–3.58	0.02

Table 13. The number of days of different flood recurrence intervals of the Red River at Fargo.

Period	2026 to 2035			
Scenario	RCP4.5 Without Flood Diversion	RCP8.5 Without Flood Diversion	RCP4.5 With Flood Diversion	RCP8.5 With Flood Diversion
10-year	161	182	172	199
50-year	27	27	4	4
100-year	17	25	0	3
500-year	0	0	0	0
Period	2036 to 2045			
Scenario	RCP4.5 Without Flood Diversion	RCP8.5 Without Flood Diversion	RCP4.5 With Flood Diversion	RCP8.5 With Flood Diversion
10-year	147	83	157	92
50-year	20	11	3	0
100-year	18	10	2	0
500-year	1	0	0	0